

Non-parabolic band hydrodynamical model of silicon semiconductors and simulation of electron devices

Vittorio Romano^{*,†}

Dipartimento Interuniversitario di Matematica, Politecnico di Bari, via E. Orabona 4-70125 Bari, Italy

Communicated by W. Allegretto

SUMMARY

A consistent hydrodynamical model for electron transport in silicon semiconductors, free of any fitting parameter, has been formulated in Anile and Romano (*Continuum Mechanics Thermodynamics* 1999; **11**:307–325) and Romano (*Continuum Mechanics Thermodynamics* 1999; **12**:31–51) on the basis of the maximum entropy principle, by considering the energy band described by the Kane dispersion relation. Explicit constitutive functions for fluxes and production terms in the macroscopic balance equations of density, crystal momentum, energy and energy flux have been obtained. Scatterings of electrons with non-polar optical phonons (both for intervalley and intravalley interactions), acoustic phonons and impurities have been taken into account.

In this article we show the link with other macroscopic models describing the motion of charge carriers. In particular, under suitable scaling assumptions, an energy transport model is recovered. An analysis of the formal properties is given by showing that the evolution equations form a hyperbolic system in the physically relevant region of the space of the dependent variables. At last, by using the numerical method developed in Liotta *et al.* (*International Series of Numerical Mathematics* 1999; **130**:651–660) and Liotta *et al.* (*SIAM Journal on Numerical Analysis* 1999, to appear) simulations for bulk silicon and $n^+ - n - n^+$ silicon diode are performed. The obtained results are in good agreement with the Monte Carlo data. Copyright © 2001 John Wiley & Sons, Ltd.

KEY WORDS: semiconductors, hydrodynamical models for charge transport, hyperbolic system, numerical methods for conservation law

1. INTRODUCTION

The simulation of submicron electron devices by directly integrating the semiclassical electron transport equation is a daunting computational task. This has prompted the development of macroscopic models for the description of charge transport in semiconductors. The main problem related to these models is that of the closure because the number of unknown functions

* Correspondence to: V. Romano, Dipartimento Interuniversitario di Matematica, Politecnico di Bari, via E. Orabona 4-70125 Bari, Italy

† E-mail: romano@dipmat.unict.it

Contract/grant sponsor: MURST, CNR Project; contract/grant number: 96.03855.CT01
Contract/grant sponsor: TMR Program; contract/grant number: ERBFMRXCT970157

exceeds that of the balance equations. In the hydrodynamical models usually employed in the applications (e.g. that proposed in References [1,2]) on the basis of heuristic arguments and in analogy with heat-conducting classical gas, ad hoc closure relations, containing free adjustable parameters, have been introduced without any justification in the framework of a consistent non-equilibrium thermodynamical theory. The resulting equations are not according to the Onsager reciprocity conditions [3] and the agreement of the numerical results with Monte Carlo data are not very accurate.

Another family of macroscopic models is represented by the energy transport (ET) models that comprise the balance equation for density and energy. They improve the standard *drift-diffusion* model [4–6], based only on the balance equation of density and upon the condition (violated in the submicron devices) of thermal equilibrium, but their formulation until now is not completely clear and free parameters are still present. The derivation given in References [7,8] is of heuristic type, while the formal derivation based on the *spherical harmonic expansion* (SHE) model (see [9] and references therein) has been obtained upon the strong and rather unphysical assumption that the dominant scattering mechanism is the electron–electron interaction. In the modern electron devices the electron density is so low that the electron–electron interaction as well as the degenerate effects can be practically neglected.

A systematic approach to the question has been followed in Reference [10] by resorting to the maximum entropy principle in the framework of the extended thermodynamics [11,12] and moment theory of Levermore [13] in the case of parabolic approximation for the electron energy bands (previous attempts in the same direction can also be found in References [3,14,15]). However, the parabolic band is too poor for realistic simulations and models with a more sophisticated description of the energy bands are warranted.

In References [16,17] the non-parabolicity effects have been consistently included. In these articles the maximum entropy principle has been employed to get consistent closure relations when the energy bands are approximated by the Kane formula and the balance equations for density, average crystal momentum, average energy and average flux of crystal momentum are considered. Since the attention is devoted to silicon semiconductors, the scattering mechanisms taken into account have been those of electrons with non-polar optical phonons, acoustic phonons and impurities of the crystal. The electron–electron scatterings as well as the degeneration effects may be neglected for the reasons mentioned above. A validation of the constitutive equations by a direct comparison with the Monte Carlo data in the bulk case [18] are very encouraging.

Here the mathematical properties of the model proposed in References [16,17] and the link with the energy transport models are investigated. Moreover, an intensive numerical integration of some test cases is presented. In particular, in bulk silicon the effects of overshoot and saturation velocity and the simulations of an $n^+n^-n^+$ diode are studied. Comparison to Monte Carlo results indicates that the model is very accurate.

The plan of the paper is as follows. In Section 2 a brief account of the electron transport in semiconductors is presented and, in particular, the basic assumptions on the scattering mechanism are given (for the notation the reader is referred to References [16,17] and for a more complete review see a standard textbook of solid-state physics, e.g. References [19–22]). In Section 3 the moment equations, the maximum entropy principle and its use for getting the desired closure relations are presented. Section 4 is devoted to recover, under an appropriate and physically reasonable scaling assumptions, an ET limit model. The mathematical properties of the model presented in References [16,17] are analysed in Section 5, by showing that

evolution equations form a quasilinear hyperbolic system in the physically relevant region of the phase space. A suitable numerical scheme is shown in Section 6 and in the last section numerical results for bulk silicon and silicon diodes are reported.

2. KINETIC DESCRIPTION

The kinetic description of the transport of electrons in semiconductors is based on the semi-classical Boltzmann transport equation (hereafter BTE). For electrons in a conduction band (the motion of holes will not be considered in the following) it reads

$$\frac{\partial f}{\partial t} + v^i(\mathbf{k}) \frac{\partial f}{\partial x^i} - \frac{eE^i}{\hbar} \frac{\partial f}{\partial k^i} = \mathcal{C}[f] \quad (1)$$

where $f(\mathbf{x}, t, \mathbf{k})$ is the one-particle distribution function giving the probability of finding an electron, in the position \mathbf{x} and at time t , with a state belonging to a small volume of the first Brillouin zone \mathcal{B} centred at the state of wave vector \mathbf{k} . $\mathcal{C}[f]$ describes the effects due to scattering with phonons, impurities and with other electrons. \mathbf{E} represents the self-consistent electric field which is related to the electron distribution function through Poisson's equation

$$\mathbf{E} = -\nabla_x \phi \quad (2)$$

$$\varepsilon \Delta \phi = -e(N_D - N_A - n) \quad (3)$$

where ϕ is the electric potential, N_D and N_A , are, respectively, the donor and acceptor densities, e the elementary charge, ε the dielectric constant and n the particle density, defined as

$$n = \int_{\mathcal{B}} f \, d^3\mathbf{k}$$

The electron group velocity \mathbf{v} is given by

$$\mathbf{v} = \frac{1}{\hbar} \nabla_{\mathbf{k}} \mathcal{E}$$

where $\mathcal{E}(\mathbf{k})$ is the energy of the considered conduction band structure of the crystal measured from the band minimum.

In the parabolic approximation the energy bands are described by

$$\mathcal{E} = \frac{\hbar^2 |\mathbf{k}|^2}{2m^*} \quad (4)$$

with m^* the effective electron mass (for silicon $m^* = 0.32m_e$, with m_e the electron mass in vacuum), $\hbar\mathbf{k}$ the *crystal momentum*, which is assumed to vary for consistency in all \mathcal{R}^3 , and \hbar the Planck constant h divided by 2π . However at high energy the parabolic approximation is rather unsatisfactory.

The Kane dispersion relation considerably improves the parabolic approximation, particularly at high energy. In this case \mathcal{E} still depends only on k , the modulus of \mathbf{k} , but

$$\mathcal{E}(k) [1 + \alpha \mathcal{E}(k)] = \frac{\hbar^2 k^2}{2m^*}, \quad \mathbf{k} \in \mathcal{R}^3 \quad (5)$$

where α is the non-parabolicity parameter.

Concerning the collision term, the main scattering mechanisms in a silicon semiconductor are the electron–phonon interaction, the interaction with impurities, electron–electron scatterings and interaction with stationary imperfections of the crystal as vacancies, external and internal crystal boundaries. The electron–electron scattering is important only at densities higher than those encountered in electron devices. Therefore it will not be taken into account. The scattering with impurities, imperfections and vacancies will not be considered as well.

In general, the collision operator for each type of interaction can be schematically written as

$$\mathcal{C}[f] = \int_{\mathcal{B}} [P(\mathbf{k}', \mathbf{k})f(\mathbf{k}') - P(\mathbf{k}, \mathbf{k}')f(\mathbf{k})] d^3\mathbf{k}' \quad (6)$$

with $P(\mathbf{k}, \mathbf{k}')$ the transition probability per unit time from a state \mathbf{k} to a state \mathbf{k}' . The first term in (6) represents the gain and the second one the loss.

In silicon electron–phonon scatterings are of elastic and inelastic types [20,21]. In the case of elastic scattering the transition probability can be written as

$$P(\mathbf{k}, \mathbf{k}') = \frac{k_B T_L \Xi_d^2}{4\pi^2 \hbar \rho v_s^2} \delta(\mathcal{E} - \mathcal{E}') \quad (7)$$

where δ is the Dirac delta function, Ξ_d the acoustic-phonon deformation potential, ρ the mass density of the material and v_s the sound velocity of the longitudinal acoustic mode and T_L the lattice temperature which will be taken as constant in the following. In the case of inelastic scattering the transition probability is constituted by the absorption and emission term:

$$P(\mathbf{k}, \mathbf{k}') = Z_f \frac{(D_t K)^2}{8\pi^2 \rho \omega} [n_B \delta(\mathcal{E}' - \mathcal{E} - \hbar\omega) + (n_B + 1) \delta(\mathcal{E}' - \mathcal{E} + \hbar\omega)] \quad (8)$$

where Z_f is the number of final equivalent valleys in the intervalley scattering, $D_t K$ is the deformation potential for optical phonons, $\hbar\omega$ is the longitudinal optical phonon energy and n_B is the phonon equilibrium distribution according to the Bose–Einstein statistics

$$n_B = \frac{1}{\exp(\hbar\omega/k_B T_L) - 1}$$

In silicon the electrons that mainly contribute to the transport properties are those in lowest energy band, that can be considered as constituted by six equivalent valleys around the minima located near the X points in the $\langle 100 \rangle$ crystallographic directions. Therefore, the general expression of the collision terms is

$$\mathcal{C}[f] = \mathcal{C}^{(\text{elastic})}[f] + \sum_{A=1}^6 \mathcal{C}_A^{(\text{inelastic})}[f].$$

In Tables I and II we summarize the values of the physical parameters and coupling constants relative to each valley.

In Reference [17] a more complicated model for the transition probability has been also considered. However, as indicated in References [20,21] the model presented above, even if it is simpler, is considered as the more accurate one.

Table I. Values of the physical parameters used for silicon.

m_e	Electron rest mass	9.1095×10^{-28} g
m^*	Effective electron mass	$0.32 m_e$
T_L	Lattice temperature	300 K
ρ	Density	2.33 g/cm ³
v_s	Longitudinal sound speed	9.18×10^5 cm/s
Ξ_d	Acoustic-phonon deformation potential	9 eV
α	Non-parabolicity factor	0.5 eV^{-1}
ε_r	Relative dielectric constant	11.7
ε_0	Vacuum dielectric constant	8.85×10^{-18} C/V μm

Table II. Coupling constants and phonon energies for the inelastic scatterings in silicon.

A	Z_f	$\hbar\omega$ (meV)	$D_f K$ (10^8 eV/cm)
1	1	12	0.5
2	1	18.5	0.8
3	4	19.0	0.3
4	4	47.4	2.0
5	1	61.2	11
6	4	59.0	2.0

3. THE MOMENT EQUATIONS

The direct attempts to solve the system of the BTE coupled to Poisson equation, meet with daunting computational difficulties and indeed, in general, solutions are available only in a stochastic sense and have been obtained by the Monte Carlo simulations. This has prompted the development of continuum model, more practical for CAD use.

The macroscopic balance equations are deduced as moment equations of the Boltzmann transport equation like in gasdynamics by multiplying Equation (1) by a function $\psi(\mathbf{k})$ and integrating over \mathcal{B} .

In the applications several choices of the weight function ψ can be made and they lead to different balance equations for macroscopic quantities. For time-dependent simulation a convenient choice [17] is 1, $\hbar\mathbf{k}$, \mathcal{E} and $\mathcal{E}\mathbf{v}$.

By considering such expressions for ψ one obtains the continuity equation (indeed a term due to the generation–recombination mechanism should appear on the right-hand side, but this effect is relevant for times of order 10^{-9} s and in most applications can be neglected because the characteristic times are of the order of a fraction of picosecond), the balance equation for the crystal momentum, the balance equation for the electron energy and the balance equation for the electron energy flux.

This set of balance equations reads as

$$\frac{\partial n}{\partial t} + \frac{\partial(nV^i)}{\partial x^i} = 0 \quad (9)$$

$$\frac{\partial(nP^i)}{\partial t} + \frac{\partial(nU^{ij})}{\partial x^j} + neE^i = nC_P^i \quad (10)$$

$$\frac{\partial(nW)}{\partial t} + \frac{\partial(nS^j)}{\partial x^j} + neV_k E^k = nC_W \quad (11)$$

$$\frac{\partial(nS^i)}{\partial t} + \frac{\partial(nF^{ij})}{\partial x^j} + neE_j G^{ij} = nC_W^i \quad (12)$$

where

$$n = \int_{\mathcal{R}^3} f \, d^3\mathbf{k} \text{ is the electron density}$$

$$V^i = \frac{1}{n} \int_{\mathcal{R}^3} f v^i \, d^3\mathbf{k} \text{ is the average electron velocity}$$

$$W = \frac{1}{n} \int_{\mathcal{R}^3} \mathcal{E}(k) f \, d^3\mathbf{k} \text{ is the average electron energy}$$

$$S^i = \frac{1}{n} \int_{\mathcal{R}^3} f v^i \mathcal{E}(k) \, d^3\mathbf{k} \text{ is the energy flux}$$

$$P^i = \frac{1}{n} \int_{\mathcal{R}^3} f \hbar k^i \, d^3\mathbf{k} = m^*(V^i + 2\alpha S^i) \text{ is the average crystal momentum}$$

$$U^{ij} = \frac{1}{n} \int_{\mathcal{R}^3} f v^i \hbar k^j \, d^3\mathbf{k} \text{ is the flux of crystal momentum}$$

$$G^{ij} = \frac{1}{n} \int_{\mathcal{R}^3} \frac{1}{\hbar} f \frac{\partial}{\partial k_j} (\mathcal{E} v_i) \, d^3\mathbf{k}$$

$$F^{ij} = \frac{1}{n} \int_{\mathcal{R}^3} f v^i v^j \mathcal{E}(k) \, d^3\mathbf{k} \text{ is the flux of energy flux}$$

$$C_P^i = \frac{1}{n} \int_{\mathcal{R}^3} \mathcal{C}[f] \hbar k^i \, d^3\mathbf{k} \text{ is the production of the crystal momentum balance equation}$$

$$C_W = \frac{1}{n} \int_{\mathcal{R}^3} \mathcal{C}[f] \mathcal{E}(k) \, d^3\mathbf{k} \text{ is the production of the energy balance equation}$$

$$C_W^i = \frac{1}{n} \int_{\mathcal{R}^3} \mathcal{C}[f] v^i \mathcal{E}(k) \, d^3\mathbf{k} \text{ is the production of the energy flux balance equation}$$

In order to simplify the algebra in the following we will often substitute Equation (10) with a linear combination of Equations (10) and (12)

$$\frac{\partial}{\partial t} nm^* V^i + \frac{\partial}{\partial x^j} [n(U_{ij} - 2\alpha m^* F_{ij})] + neE^i(1 - 2\alpha m^* G_{ij}) = n(C_p^i - 2\alpha m^* C_w^i) \quad (13)$$

4. THE MAXIMUM ENTROPY PRINCIPLE AND CLOSURE RELATIONS

The moment equations do not constitute a set of closed relations because of the fluxes and production terms. Therefore constitutive assumptions must be prescribed.

If we assume as fundamental variables n, V^i, W and S^i , which have a direct physical interpretation, the closure problem consists in expressing P^i, U^{ij}, F^{ij} and G^{ij} and the moments of the collision term, C_p^i, C_w and C_w^i , as functions of n, V^i, W and S^i .

The *maximum entropy principle* (hereafter MEP) leads to a systematic way for obtaining constitutive relations on the basis of information theory (see References [11–13,23] for a review).

According to the MEP if a given number of moments M_A are known, the distribution function f_{ME} which can be used to evaluate the unknown moments of f , corresponds to the extremal of the entropy functional under the constraints that it yields exactly the known moments M_A

$$\int_{\mathcal{R}^3} \psi_A f_{ME} d^3 \mathbf{k} = M_A \quad (14)$$

Since the electrons interact with the phonons describing the thermal vibrations of the ions placed at the points of the crystal lattice, in principle, we should deal with a two-component system (electrons and phonons). However, if one consider the phonon gas as a thermal bath at constant temperature T_L , only the electron component of the entropy must be maximized. Moreover, by considering the electron gas as sufficiently dilute, one can take for the electron gas the expression of the entropy obtained as the Maxwellian limiting case of that arising from the Fermi statistics

$$s = -k_B \int_{\mathcal{R}^3} (f \log f - f) d^3 \mathbf{k} \quad (15)$$

If we introduce the Lagrangian multipliers Λ_A , the problem to maximize s under constraint (14) is equivalent to maximize

$$s' = \Lambda^A M_A - s$$

the Legendre transform of s , without constraints. This gives

$$f_{ME} = \exp \left[-\frac{1}{k_B} \Lambda_A \psi^A \right] \quad (16)$$

If n, V^i, W and S^i are assumed as fundamental variables, then

$$\psi^A = (1, \mathbf{v}, \mathcal{E}, \mathcal{E}\mathbf{v})$$

and

$$\Lambda_A = (\lambda, k_B \lambda_i, k_B \lambda^W, k_B \lambda_i^W)$$

with λ being the Lagrangian multiplier relative to the density n , λ^W the Lagrangian multiplier relative to the energy W , λ_i the Lagrangian multiplier relative to the velocity V^j and λ_i^W the Lagrangian multiplier relative to the energy flux S^j .

In order to get the dependence of the Λ_A 's from the M_A , one has to invert the constraints (14).

Now at equilibrium the distribution function is isotropic

$$f_{\text{EQ}} = \exp \left[- \left(\frac{1}{k_B} \lambda_E + \frac{\mathcal{E}}{k_B T_L} \right) \right] \quad (17)$$

that is at equilibrium

$$\lambda_E^W = \frac{1}{k_B T_L}, \quad \lambda_E^i = 0, \quad \lambda_E^{iW} = 0$$

the Monte Carlo simulations for electron transport in Si show that the anisotropy of f is small [24, 25] even far from equilibrium.

Upon such a consideration we make the ansatz of small anisotropy for f_{ME} . Formally, we introduce a *small* anisotropy parameter δ , assume that the multipliers are analytic in δ and expand them around $\delta=0$ by taking into account the representation theorems for isotropic functions.

Explicit expressions for the Lagrangian multipliers have been achieved up to second-order terms in References [16, 17]. Here we will employ only the linear model (up to first order in δ). As the results of the simulation will show, it is already sufficiently accurate while, in the parabolic case, the inclusion of quadratic terms gave rise in Reference [10] to irregularities in the solutions.

Once f_{ME} has been obtained, one can insert it into the definitions of the unknown quantities and get the desired constitutive relations.

Up to first-order terms the constitutive equations for fluxes are of the form

$$U_{ij} = U^{(0)} \delta_{ij}, \quad F_{ij} = F^{(0)} \delta_{ij}, \quad G_{ij} = G^{(0)} \delta_{ij} \quad (18)$$

The explicit form of $U^{(0)}, F^{(0)}$ and $G^{(0)}$ are given in References [16, 17]. In the parabolic band approximation ($\alpha=0$) one finds

$$U_{ij}^{\text{P}} = \frac{2}{3} W \delta_{ij}, \quad m^{\star} F_{ij}^{\text{P}} = \frac{10}{9} W^2 \delta_{ij}, \quad m^{\star} G_{ij} = \frac{5}{3} W \delta_{ij} \quad (19)$$

Similarly, it is possible to evaluate the production terms.

For the collision term of elastic phonon scattering one gets

$$C_W = 0$$

while the production terms of crystal momentum and energy flux can be put in the form

$$C_P^i = c_{11}^{(\text{ac})}(W)V_i + c_{12}^{(\text{ac})}(W)S_i \quad (20)$$

$$C_W^i = c_{21}^{(\text{ac})}(W)V_i + c_{22}^{(\text{ac})}(W)S_i \quad (21)$$

The production matrix $C^{(\text{ac})} = (c^{(\text{ac})})$, is given in Reference [7].

For inelastic phonon scattering, the energy is no longer conserved,

$$C_W \leq 0$$

and $C_W = 0$ only for $W = W_0$, with $W_0 = 3/2k_B T_L$ the equilibrium energy (see Reference [17]), while the production terms of crystal momentum and energy flux have again the form (see Reference [17])

$$C_P^i = c_{11}^{(\text{np})}(W)V_i + c_{12}^{(\text{np})}(W)S_i \quad (22)$$

$$C_W^i = c_{21}^{(\text{np})}(W)V_i + c_{22}^{(\text{np})}(W)S_i \quad (23)$$

For the sake of completeness we summarize in the appendix all the constitutive equations.

5. THE ENERGY TRANSPORT LIMIT MODEL

Other macroscopic models, simpler than the hydrodynamical models but more accurate than the *drift-diffusion* ones [6], are constituted by the *energy transport* (ET) models, which are based on the balance equations for density and energy. The ET models currently employed in the device simulation, have been derived in References [7, 8] in a semiheuristic way. A more formal derivations has been proposed starting on the spherical harmonic expansion (SHE) model (see [9] and references therein) under the basic assumption that the dominant scattering mechanism is the electron–electron one. However, this scaling has a rather dubious physical validity since in the situation encountered in the applications the electron density is instead very low so that the degeneracy effects and consistently the electron–electron interactions are usually neglected in almost all the electron device simulations even if Monte Carlo techniques are employed [24, 26].

Here we derive from the hydrodynamical model presented in the previous section an energy transport model as asymptotic limit under physically more appropriate scaling assumptions.

We assume that the following scaling holds (for the sake of simplicity in the notation we continue to denote scaled and original variables with the same symbol)

$$t = \mathcal{O}\left(\frac{1}{\delta^2}\right), \quad x^i = \mathcal{O}\left(\frac{1}{\delta}\right), \quad \mathbf{V} = \mathcal{O}(\delta), \quad \mathbf{S} = \mathcal{O}(\delta), \quad \tau_W = \mathcal{O}\left(\frac{1}{\delta^2}\right) \quad (24)$$

where τ_W is the energy relaxation time, defined as

$$C_W = -\frac{W - W_0}{\tau_W}$$

with W_0 energy at equilibrium. The symbol $\mathcal{O}(\cdot)$ means, as usual, quantity of order (\cdot) .

Relation (24)₁ means a long time scaling, while the (24)₂ indicates a diffusion approximation. Assumptions (24)₃ and (24)₄ are consistent with the small anisotropy condition in the derivation of the f_{ME} , while relation (24)₅ means that the energy must relax to equilibrium slower than the velocity and energy flux.

The following proposition gives the ET limiting model deduced from the hydrodynamical model (9)–(12).

Proposition 5.1. Under the scaling assumption (24), for smooth solutions, the following compatibility conditions arise from system (9)–(12)

$$\frac{\partial n}{\partial t} + \frac{\partial(nV^i)}{\partial x^i} = 0 \tag{25}$$

$$\frac{\partial(nW)}{\partial t} + \frac{\partial(nS^j)}{\partial x^j} + neV_k E^k = nC_W \tag{26}$$

with

$$V^i = D_{11}(W) \frac{\partial}{\partial x^i} \log n + D_{12}(W) \frac{\partial}{\partial x^i} W + D_{13}(W) \frac{\partial}{\partial x^i} \phi \tag{27}$$

$$S^i = D_{21}(W) \frac{\partial}{\partial x^i} \log n + D_{22}(W) \frac{\partial}{\partial x^i} W + D_{23}(W) \frac{\partial}{\partial x^i} \phi \tag{28}$$

The elements of the diffusion matrix $D = (D_{ij})$ are given by

$$D_{11} = \frac{c_{22}U^{(0)} - c_{12}F^{(0)}}{c_{11}c_{22} - c_{12}c_{21}}, \quad D_{12} = \frac{c_{22}U^{(0)'} - c_{12}F^{(0)'}}{c_{11}c_{22} - c_{12}c_{21}}, \quad D_{13} = -e \frac{c_{22} - c_{12}G^{(0)}}{c_{11}c_{22} - c_{12}c_{21}} \tag{29}$$

$$D_{21} = \frac{c_{11}F^{(0)} - c_{21}U^{(0)}}{c_{11}c_{22} - c_{12}c_{21}}, \quad D_{22} = \frac{c_{11}F^{(0)'} - c_{21}U^{(0)'}}{c_{11}c_{22} - c_{12}c_{21}}, \quad D_{23} = e \frac{c_{21} - c_{11}G^{(0)}}{c_{11}c_{22} - c_{12}c_{21}} \tag{30}$$

The prime denotes derivative with respect to W .

Proof. We shall proceed in a formal way. Assumption (24)₂ and relation (2) between the electric field and the electric potential imply $\mathbf{E} = \mathcal{O}(\delta)$. By including scaling (24) into system (9)–(12), we have been observing that C_p^i and C_W^i are of the order δ ,

$$\delta^2 \left[\frac{\partial n}{\partial t} + \frac{\partial(nV^i)}{\partial x^i} \right] = 0$$

$$\begin{aligned} \delta^3 \frac{\partial(nP^i)}{\partial t} + \delta \left[\frac{\partial(nU^{ij})}{\partial x^j} + neE^i - nC_P^i \right] &= 0 \\ \delta^2 \left[\frac{\partial(nW)}{\partial t} + \frac{\partial(nS^j)}{\partial x^j} + neV_k E^k - nC_W \right] &= 0 \\ \delta^2 \frac{\partial(nS^i)}{\partial t} + \delta \left[\frac{\partial(nF^{ij})}{\partial x^j} + neE_j G^{ij} - nC_W^i \right] &= 0 \end{aligned}$$

and by putting equal to zero the coefficients of the various powers of δ in the previous system, one gets again the balance equations (25) and (26) of density and energy and, moreover,

$$\begin{aligned} \frac{\partial}{\partial t} nV^i &= 0, \quad \frac{\partial}{\partial t} nS^i = 0 \\ \frac{1}{n} \frac{\partial}{\partial x^j} nU^{(0)} &= -eE^i + c_{11}V^i + c_{12}S^i \\ \frac{1}{n} \frac{\partial}{\partial x^j} nF^{(0)} \delta_{ij} &= -eE^i G^{(0)} + c_{21}V^i + c_{22}S^i \end{aligned}$$

The last two relations allow to express \mathbf{V} and \mathbf{S} as functions of n , W and ϕ and give (27) and (28) by a simple computation. \square

Remark 5.1. In the stationary case the original model (9)–(12) and the limiting ET one (25)–(28) are equivalent, at least for smooth solutions.

Remark 5.2. At variance with the above-quoted references on the ET models [7–9], we use W as variable and not the temperature. In fact, the definition of a non-equilibrium temperature in the context of non-equilibrium thermodynamics is itself a controversial question. For the problem of electron transport in the parabolic band approximation the analogy with the monoatomic gas gives an indication about the definition of temperature (see References [16, 17]). When the Kane dispersion relation is employed there is no such analogy and the introduction of the concept of non-equilibrium temperature becomes very questionable, mainly for the physical interpretation when comparisons with measurements are made.

Remark 5.3. From a mathematical point of view the two balance equations of the resulting ET model for the density and the energy constitute a parabolic system of PDEs. In fact, in Figure 1 we have plotted the eigenvalues of the matrix

$$\hat{D} = \begin{pmatrix} D_{11} & D_{12} \\ D_{21} & D_{22} \end{pmatrix}$$

for values of W of interest in the applications. In the considered range of energies, the matrix \hat{D} is negative definite.

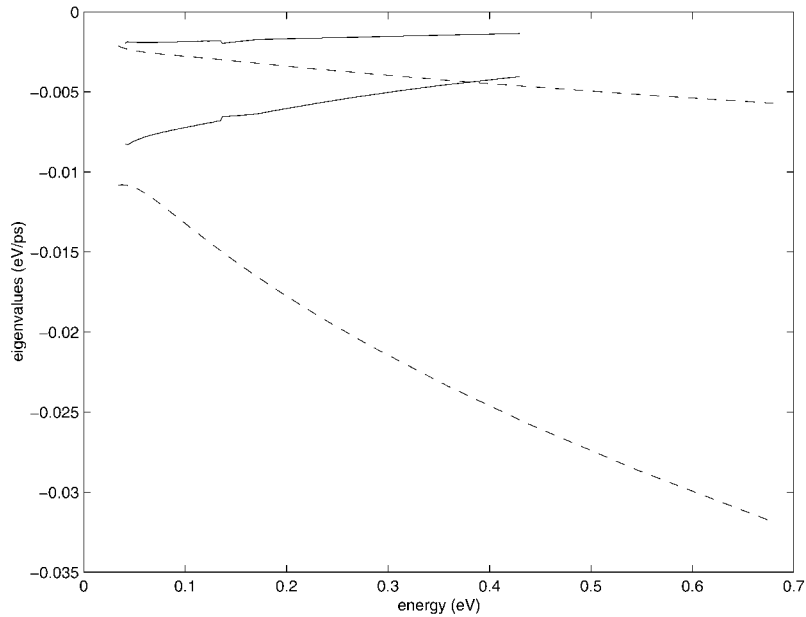


Figure 1. The eigenvalues of the matrix \hat{D} versus the energy W (eV) in the parabolic case (dashed line) and for the Kane dispersion relation (continuous line).

In stationary case the two balance equations (25)–(26) supplemented by the Poisson equation form an elliptic system of PDEs.

6. THE FORMAL PROPERTIES OF THE HYDRODYNAMICAL MODEL

In this section we will investigate the formal properties of system (9)–(12). We will prove that it forms a hyperbolic system in the physically relevant region of the space of the dependent variables.

Let us consider the quasi-linear system of PDEs

$$\frac{\partial}{\partial t} F^{(0)}(\mathbf{U}) + \sum_{i=1}^3 \frac{\partial}{\partial x^i} F^{(i)}(\mathbf{U}) = B(\mathbf{U}) \quad (31)$$

with

$$F : \Omega \mapsto \mathcal{R}^m$$

sufficiently smooth function and $\Omega \subset \mathcal{R}^m$. If we consider a smooth solution, we can introduce the Jacobian matrices

$$A^{(\beta)} = \nabla_{\mathbf{U}} F^{(\beta)}, \quad \beta = 0, 1, 2, 3$$

We recall that system (31) is said *hyperbolic in the t-direction* if $\det(A^{(0)}(\mathbf{U})) \neq 0$ and the eigenvalues problem

$$\det\left(\sum_{i=1}^3 n_i A^{(i)}(\mathbf{U}) - \lambda A^{(0)}(\mathbf{U})\right) = 0 \tag{32}$$

has real eigenvalues and the eigenvectors span \mathcal{R}^m for all unit vectors $\mathbf{n} = (n_1, n_2, n_3)$.

In the case of system (9), (11)–(13) we have

$$\mathbf{U} = \begin{pmatrix} n \\ V^1 \\ V^2 \\ V^3 \\ W \\ S^1 \\ S^2 \\ S^3 \end{pmatrix}, \quad F^{(0)} = n \begin{pmatrix} 1 \\ m^* V^1 \\ m^* V^2 \\ m^* V^3 \\ W \\ S^1 \\ S^2 \\ S^3 \end{pmatrix}$$

$$F^{(1)} = n \begin{pmatrix} V^1 \\ (U - 2\alpha m^* F) \\ 0 \\ 0 \\ S^1 \\ nF \\ 0 \\ 0 \end{pmatrix}, \quad F^{(2)} = n \begin{pmatrix} V^2 \\ 0 \\ (U - 2\alpha m^* F) \\ 0 \\ S^2 \\ 0 \\ nF \\ 0 \end{pmatrix}, \quad F^{(3)} = n \begin{pmatrix} V^3 \\ 0 \\ 0 \\ (U - 2\alpha m^* F) \\ S^3 \\ 0 \\ 0 \\ nF \end{pmatrix}$$

and the Jacobian matrices are given by

$$A^{(0)} = \begin{pmatrix} 1 & 0 & 0 & 0 & 0 & 0 & 0 & 0 \\ m^* V^1 & m^* n & 0 & 0 & 0 & 0 & 0 & 0 \\ m^* V^2 & 0 & m^* n & 0 & 0 & 0 & 0 & 0 \\ m^* V^3 & 0 & 0 & m^* n & 0 & 0 & 0 & 0 \\ W & 0 & 0 & 0 & n & 0 & 0 & 0 \\ S^1 & 0 & 0 & 0 & 0 & n & 0 & 0 \\ S^2 & 0 & 0 & 0 & 0 & 0 & n & 0 \\ S^3 & 0 & 0 & 0 & 0 & 0 & 0 & n \end{pmatrix}$$

$$A^{(n)} = \sum_{i=1}^3 n_i A^{(i)}$$

$$= \begin{pmatrix} n_k V^k & n_1 n & n_2 n & n_3 n & 0 & 0 & 0 & 0 \\ n_1(U - 2\alpha m^* U) & 0 & 0 & 0 & n_1 n(U' - 2\alpha m^* F') & 0 & 0 & 0 \\ n_2(U - 2\alpha m^* U) & 0 & 0 & 0 & n_2 n(U' - 2\alpha m^* F') & 0 & 0 & 0 \\ n_3(U - 2\alpha m^* U) & 0 & 0 & 0 & n_3 n(U' - 2\alpha m^* F') & 0 & 0 & 0 \\ n_k S^k & 0 & 0 & 0 & 0 & n_1 n & n_2 n & n_3 n \\ n_1 F & 0 & 0 & 0 & n_1 n F' & 0 & 0 & 0 \\ n_2 F & 0 & 0 & 0 & n_2 n F' & 0 & 0 & 0 \\ n_3 F & 0 & 0 & 0 & n_3 n F' & 0 & 0 & 0 \end{pmatrix}$$

where the prime denote partial derivation with respect to W .

Let us introduce the region $\hat{\Omega} = \{\mathbf{U} \in \mathcal{R}^8 : n > 0, W > 0\}$ and the functions

$$g_1(W) = (U + m^* F' - WU' + 2\alpha m^*(WF' - F))^2 - 4m^*(UF' - U'F) \tag{33}$$

$$g_2(W) = U + m^* F' - WU' + 2\alpha m^*(WF' - F) - \sqrt{g_1(W)} \tag{34}$$

$$g_3(W) = (U - 2\alpha m^* F)F' - (U' - 2\alpha m^* F')F \tag{35}$$

Proposition 6.2. If the inequalities

$$g_1(W) > 0, \quad g_2(W) > 0, \quad g_3(W) > 0 \tag{36}$$

are satisfied, in the region $\hat{\Omega}$ system (9), (11)–(13) is hyperbolic.

Proof. For $\mathbf{U} \in \hat{\Omega}$ one has

$$\det(A^{(0)}) = (m^*)^3 n^7 > 0$$

In order to check the second condition of hyperbolicity, after some algebra one finds that the eigenvalues are given by

$$\lambda_{1,2,3,4} = 0 \tag{37}$$

$$\lambda_{\pm\pm} = \pm \frac{\sqrt{2}}{2} \{U + m^* F' - WU' + 2\alpha m^*(WF' - F) \pm [(U + m^* F' - WU' + 2\alpha m^*(WF' - F))^2 - 4m^*(UF' - U'F)]^{1/2}\}^{1/2} \tag{38}$$

If inequalities (36)₁ and (36)₂ are satisfied, the eigenvalues $\lambda_{\pm\pm}$ are real, distinct and different from zero. Then the hyperbolicity is guaranteed if the dimension of the kernel of $A^{(n)}$ is four.

Since $\mathbf{n} \cdot \mathbf{n} = 1$, at least one of the component n_j is different from zero. Let us suppose that $n_1 \neq 0$ and consider the submatrix of $A^{(n)}$

$$\hat{A} = \begin{pmatrix} n_k V^k & n_1 n & 0 & 0 \\ n_1(U - 2\alpha m^* F) & 0 & n_1 n(U' - 2\alpha m^* F') & 0 \\ n_k S^k & 0 & 0 & n_1 n \\ n_1 F & 0 & n_1 n F' & 0 \end{pmatrix}$$

The determinant of \hat{A} is given by

$$n_1^6 n^3 g_3(W)$$

If either n_2 or n_3 is different from zero we get the previous result with n_1 substituted by either n_2 or n_3 . Under the condition $g_3(W) > 0$ the eigenspace associated with $\lambda = 0$ has four independent eigenvectors in $\hat{\Omega}$.

Remark 6.1. In the two-dimensional case a similar analysis leads again to Proposition 5.1. The same happens in the one-dimensional case, but this time the system becomes strictly hyperbolic with eigenvalues $\lambda_{\pm\pm}$.

Remark 6.2. Now let us check conditions (36). In the parabolic band limit one has

$$g_1(W) = \frac{160}{81} W^2, \quad g_2(W) = \frac{4}{9}(5 - \sqrt{10})W, \quad g_3(W) = \frac{20}{27} W^2$$

and conditions (36) are trivially satisfied in $\hat{\Omega}$. The eigenvalues are

$$\lambda_{1,2,3,4} = 0 \quad \text{and} \quad \lambda_{\pm\pm} = \pm \sqrt{(10 \pm 2\sqrt{10})}W \quad (39)$$

In the case of the Kane dispersion relation we have numerically evaluated the function $g_1(W)$, $g_2(W)$ and $g_3(W)$ for the range of values of W typically encountered in the electron devices. Figure 2 shows that relations (36) are satisfied also in the non-parabolic case.

Therefore, we can conclude that *at least for the values of W of practical interest system (9), (11)–(13) is hyperbolic.*

7. NUMERICAL METHOD

Numerical integration of quasi-linear hyperbolic systems represents by itself an active research area (see References [27, 28]). It is well known that the solutions of quasi-linear systems suffer loss of regularity (e.g. formation of shocks). In the last decade several accurate high-order shock capturing schemes have been developed. However, they deal almost exclusively with homogeneous systems. In References [29, 30] a suitable numerical scheme for balance laws with (possibly stiff) source terms has been developed on the basis of the Nessyahu and Tadmor scheme [31] for homogeneous hyperbolic system and applied in References [10, 15, 32] for parabolic hydrodynamical models of semiconductors.

The same numerical scheme will be used for system (9), (11)–(13).

The complete method is based on a splitting technique, by solving separately the system with the source put equal to zero (convection step) and then solving the relaxation step

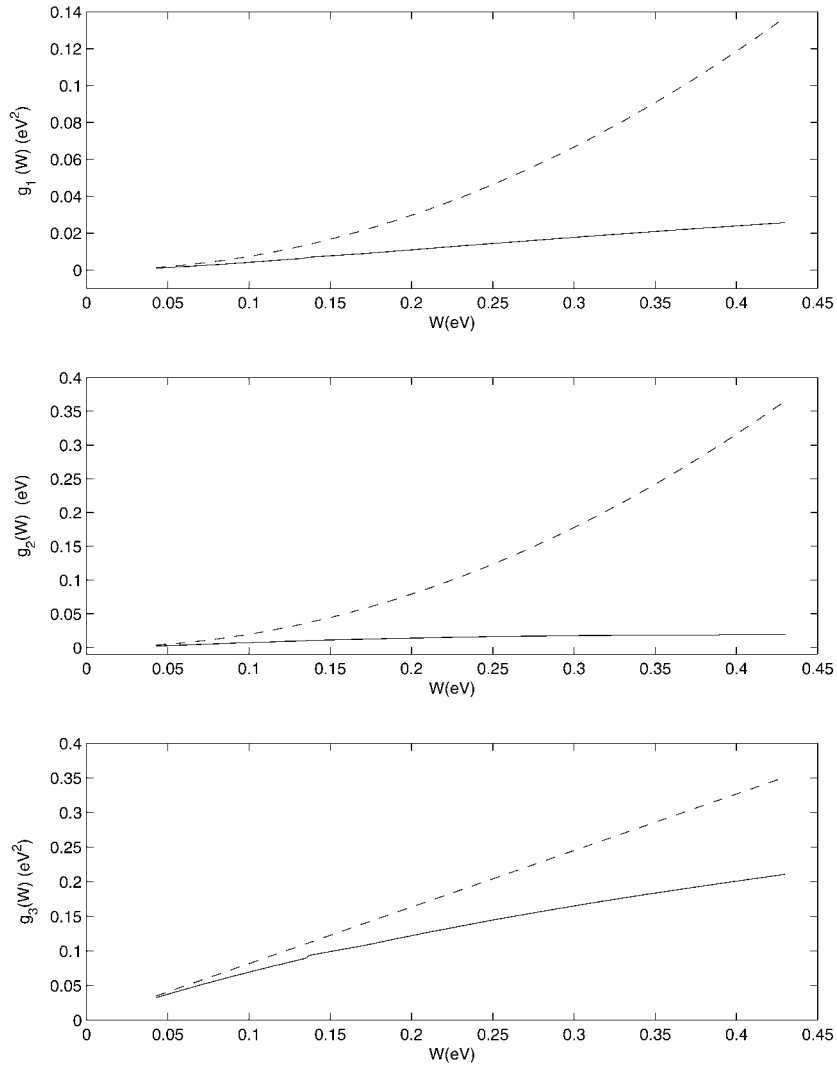


Figure 2. The functions $g_1(W)$, $g_2(W)$ and $g_3(W)$ versus the energy W (eV) in the parabolic case (dashed line) and for the Kane dispersion relation (continuous line).

(with the flux put equal to zero). A second-order accurate scheme is achieved with a suitable combination of convective and relaxation steps.

Since one-dimensional problems will be considered in the next section, we present only the one-dimensional version of the scheme.

Let us consider system (31) in the one-dimensional case

$$\frac{\partial}{\partial t} \mathbf{U} + \frac{\partial}{\partial x^i} F(\mathbf{U}) = B(\mathbf{U}, \mathbf{E}) \tag{40}$$

where $F = F^{(1)}$.

Each convective step has the form of predictor–corrector scheme [30] on a staggered grid:

$$\mathbf{U}_{j+1/2}^{n+1} = \frac{1}{2}(\mathbf{U}_j^n + \mathbf{U}_{j+1}^n) + \frac{1}{8}(\mathbf{U}_j' - \mathbf{U}_{j+1}') - \lambda[F(\mathbf{U}_{j+1}^{n+1/2}) - F(\mathbf{U}_j^{n+1/2})] \quad (41)$$

$$\mathbf{U}_j^{n+1/2} = \mathbf{U}_j^n - \frac{\lambda}{2}F_j' \quad (42)$$

where $\lambda = \Delta t/\Delta x$. The time step Δt must satisfy a stability condition

$$\lambda \max \rho(A(\mathbf{U}(x, t))) < \frac{1}{2} \quad (43)$$

where $\rho(A(v(x, t)))$ is the spectral radius of the Jacobian matrix,

$$A = \frac{\partial F}{\partial \mathbf{U}}$$

This condition will ensure that the generalized Riemann problems with piecewise smooth data at time t_n will not interfere during the time step Δt .

In order to couple the convection step with the relaxation step, it is convenient to make two convection steps of step size $\Delta t/2$, so that the solution is computed on the same grid. A complete convection step of step size Δt is obtained as a sequence of two intermediate steps of step size $\Delta t/2$.

The values of $\mathbf{U}_j'/\Delta x$ and $F_j'/\Delta x$ are a first-order approximation of the space derivatives of the field and of the flux, computed from cell averages by using a uniform non-oscillatory reconstruction,

$$\mathbf{U}_j' = \text{MM}(d_{j-1/2}v + \frac{1}{2}\text{MM}(D_{j-1}, D_j), d_{j+1/2} - \frac{1}{2}\text{MM}(D_j, D_{j+1})) \quad (44)$$

where

$$D_j = \mathbf{U}_{j+1} - 2\mathbf{U}_j + \mathbf{U}_{j-1}$$

$$d_{j+1/2} = \mathbf{U}_{j+1} - \mathbf{U}_j$$

and

$$\text{MM}(x, y) = \begin{cases} \text{sign}(x)\min(|x|, |y|) & \text{if } \text{sign}(x) = \text{sign}(y) \\ 0 & \text{otherwise} \end{cases}$$

A similar procedure is used for computing F_j' .

The electric potential is calculated with a standard procedure by central differentiation.

The relaxation step requires to solve the system of ODEs

$$\frac{dn}{dt} = 0$$

$$\frac{dV^1}{dt} = -\frac{eE^1}{m^*} + 2\alpha eE^1 G + \left(\frac{c11}{m^*} - 2\alpha c_{21}\right)V^1 + \left(\frac{c12}{m^*} - 2\alpha c_{22}\right)S^1$$

$$\frac{dW}{dt} = -eV^1 E^1 - \frac{W - W_0}{\tau_W}$$

$$\frac{dS^1}{dt} = -eE^1 G + c_{21}V^1 + c_{22}S^1$$

By freezing the energy relaxation time, the coefficients c_{lp} and the electric field at $t = t_n$, we can integrate numerically the previous equations for each node j in a semi-implicit way as

$$n^{n+1} = n^n$$

$$V_1^{n+1} = \frac{1}{\Delta t} \left[(1 - c_{22}^n \Delta t) d_1^n + d_2^n \Delta t \left(\frac{c_{12}^n}{m^*} - 2\alpha c_{22}^n \right) \right]$$

$$W^{n+1} = \left(1 + \frac{\Delta t}{\tau_W^n} \right)^{-1} \left[W^n + \left(-eE_1^n V_1^n + \frac{W_0}{\tau_W^n} \right) \Delta t \right]$$

$$S_1^n = \frac{1}{\Delta t} \left\{ c_{21}^n d_1^n \Delta t + d_2^n \left[1 - \left(\frac{c_{11}^n}{m^*} - 2\alpha c_{21}^n \right) \Delta t \right] \right\}$$

where

$$\Delta^n = (1 - c_{22}^n \Delta t) \left[1 - \left(\frac{c_{11}^n}{m^*} - 2\alpha c_{21}^n \right) \Delta t \right] - c_{21} \left(\frac{c_{12}^n}{m^*} - 2\alpha c_{22}^n \right) (\Delta t)^2$$

$$d_1^n = V_1^n + \left(-\frac{eE_1^n}{m^*} + 2\alpha eE_1^n G^n \right) \Delta t$$

$$d_2^n = S_1^n - eE_1^n G^n \Delta t$$

It is possible to obtain second-order accuracy in time by combining the two steps according to the following scheme [29, 30]. Given the fields at time t_n , (U^n, E^n) , the fields at time t_{n+1} are obtained by

$$\mathbf{U}_1 = \mathbf{U}^n - R(\mathbf{U}_1, E_1^n, \Delta t)$$

$$\mathbf{U}_2 = \frac{3}{2}\mathbf{U}^n - \frac{1}{2}\mathbf{U}_1$$

$$\mathbf{U}_3 = \mathbf{U}_2 - R(\mathbf{U}_3, E_1^n, \Delta t)$$

$$\mathbf{U}_4 = \mathcal{C}_{\Delta t} \mathbf{U}_3$$

$$E_1^{n+1} = \mathcal{P}(\mathbf{U}_4)$$

$$\mathbf{U}^{n+1} = \mathbf{U}_4 - R(\mathbf{U}^{n+1}, E_1^{n+1}, \Delta t/2)$$

where R represents the discrete operator corresponding to the relaxation step, $\mathcal{C}_{\Delta t}$ is the discrete operator corresponding to NT scheme and $\mathcal{P}(U)$ gives the solution to Poisson's equation.

8. NUMERICAL RESULTS

In this section we test the hydrodynamical model (9), (11)–(13) in silicon semiconductors by considering first the problem of the overshoot and saturation velocity in the bulk case and then by simulating a $n^+ - n - n^+$ silicon diode that models the channel of a MOSFET.

8.1. Application to bulk silicon

The physical situation is represented by silicon semiconductors with a uniform doping concentration, we assume it to be sufficiently low so that the scatterings with impurities can be neglected. On account of the symmetry with respect to translations, the solution does not depend on the spatial variables. The continuity equation gives $n = \text{constant}$ and from the Poisson equation one finds that \mathbf{E} is also constant. Therefore, the remaining balance equations reduce to the following set of ODEs for the motion along the direction of the electric field:

$$\frac{d}{dt}V = -\frac{eE}{m^*} + \frac{2\alpha eEG}{m^*} + \left(\frac{c_{11}}{m^*} - 2\alpha c_{21}\right)V + \left(\frac{c_{12}}{m^*} - 2\alpha c_{22}\right)S \quad (45)$$

$$\frac{d}{dt}W = -eVE + C_W \quad (46)$$

$$\frac{d}{dt}S = -eEG^{(0)} + c_{21}V + c_{22}S \quad (47)$$

where V and S are the component of \mathbf{V} and \mathbf{S} along the electric field.

As initial conditions for (45)–(47) we take

$$V(0) = 0 \quad (48)$$

$$W(0) = \frac{3}{2}k_B T_L \quad (49)$$

$$S(0) = 0 \quad (50)$$

The stationary regime is reached in a few picoseconds.

The solutions of (45)–(47) for several values of the electric field are reported in Figures 3 (velocity), 4 (energy) and 5 (energy flux).

The typical phenomena of overshoot and saturation velocity are both qualitatively and quantitatively well described (see Reference [22] Figure 3.22 for a comparison with the results obtained by MC simulations).

Similar results were reported in Reference [17], but there a different modelling of the collision terms has been considered and, moreover, instead to taking into account all the intervalley and intravalley scatterings, mean values of the coupling constant Ξ and $D_i K$ have been introduced. The inclusion of all the scattering (intervalley and intravalley) mechanisms improve the results notably.

For the sake of completeness also the parabolic band case has been integrated (Figures 6–8). The differences, especially in the energy, with respect to the Kane case, confirm the opinion that the parabolic band is an oversimplification of the real band structure.

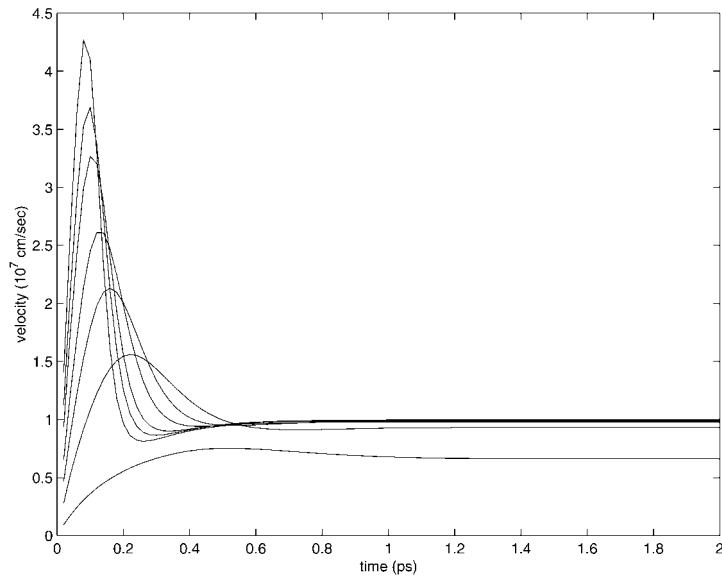


Figure 3. Velocity (cm/s) versus time (ps) for $E = 10, 30, 50, 70, 100, 120$ and 150 kV/cm.

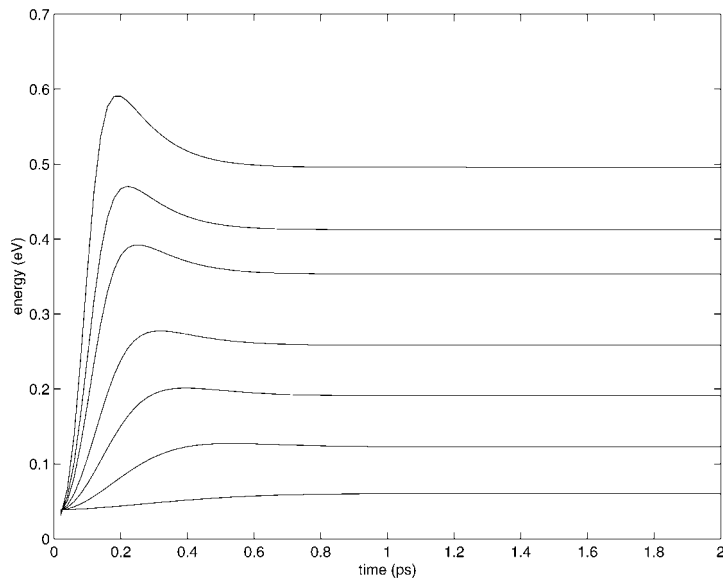


Figure 4. Energy (eV) versus time (ps) for the same values of the electric field as in Figure 3.

8.2. Application to $n^+ - n - n^+$ silicon diode

As second problem we simulate a ballistic $n^+ - n - n^+$ silicon diode. The n^+ regions are $0.1 \mu\text{m}$ long while the channel has different length. Moreover, several doping profiles will be considered according to Table III.

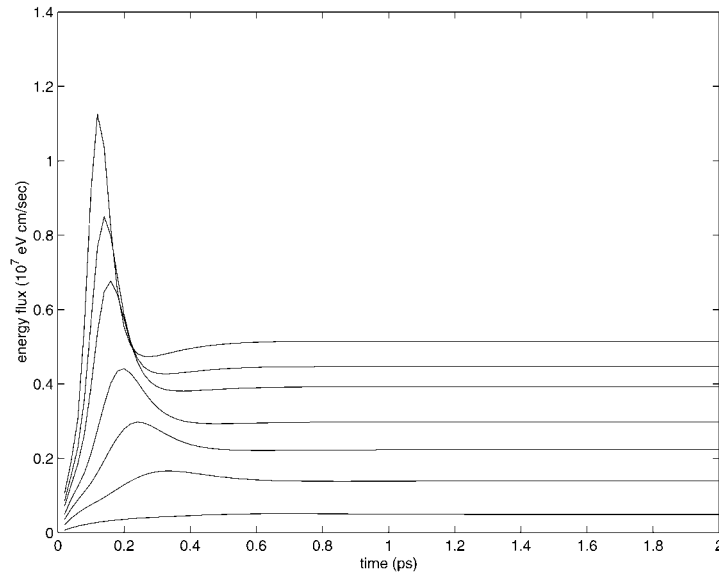


Figure 5. Energy flux (eV cm/s) versus time (ps) for the same values of the electric field as in Figure 3.

Table III. Length of the channel, doping concentration and applied voltage in the test cases for the diode.

Test #	Channel length L_c (μm)	N_D^+ ($\times 10^{17} \text{ cm}^{-3}$)	N_D ($\times 10^{17} \text{ cm}^{-3}$)	V_b (V)
1	0.4	5	0.02	2
2	0.3	10	0.1	1
3	0.2	10	0.1	1

Initially, the electron energy is that of the lattice in thermal equilibrium at the temperature T_L , the charges are at rest and the density is equal to the doping concentration

$$n(x, 0) = n_0(x), \quad W(x, 0) = \frac{3}{2} k_B T_L, \quad V(x, 0) = 0, \quad S(x, 0) = 0$$

Regarding the boundary conditions, in principle, the number of independent conditions on each boundary should be equal to the number of characteristics entering the domain. However, we impose, in analogy with similar cases [10, 33] a double number of boundary conditions. More precisely, we give conditions for all the variables in each boundary, located at $x = 0$ and L ,

$$n(0, t) = n(L, t) = N_D^+ \quad (51)$$

$$\frac{\partial}{\partial x} W(0, t) = \frac{\partial}{\partial x} W(L, t) = 0 \quad (52)$$

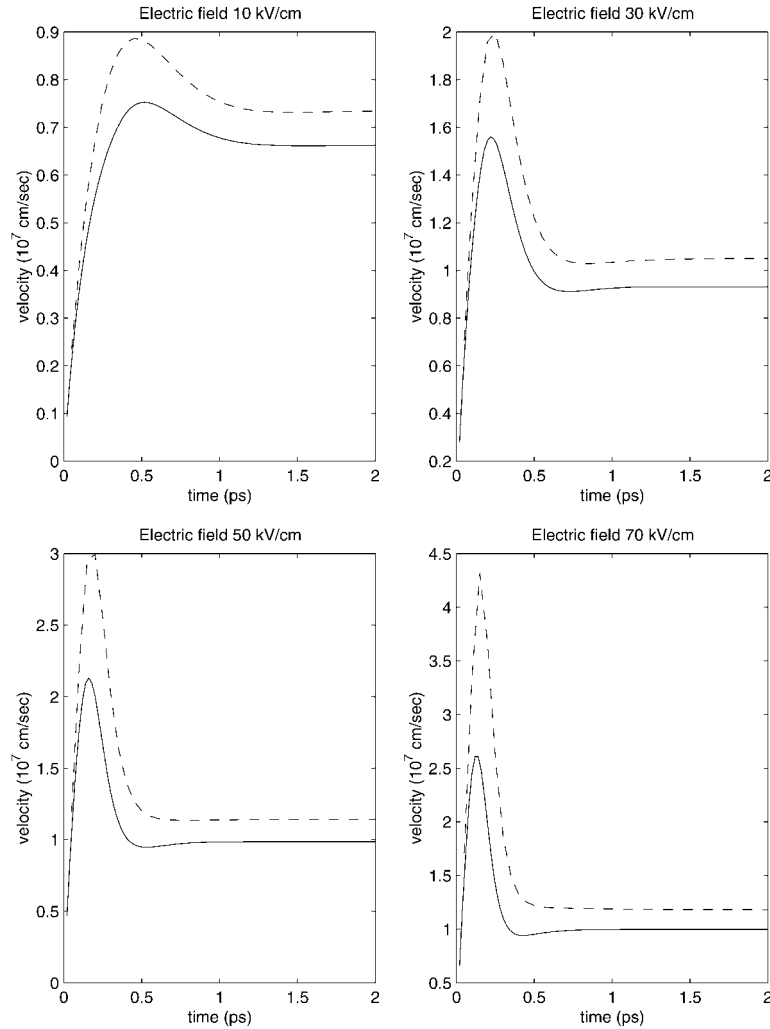


Figure 6. Velocity (cm/s) versus time (ps) in the parabolic band case (dashed line) and for the Kane dispersion relation.

$$\frac{\partial}{\partial x} V(0, t) = \frac{\partial}{\partial x} V(L, t) = 0 \tag{53}$$

$$\frac{\partial}{\partial x} S(0, t) = \frac{\partial}{\partial x} S(L, t) = 0 \tag{54}$$

$$\phi(0) = 0 \quad \text{and} \quad \phi(L) = V_b \tag{55}$$

where V_b is the applied bias voltage. In all the numerical solutions there is no sign of spurious oscillations near the boundary, indicating that conditions (51)–(54) are, in fact, compatible with the solution of the problem.

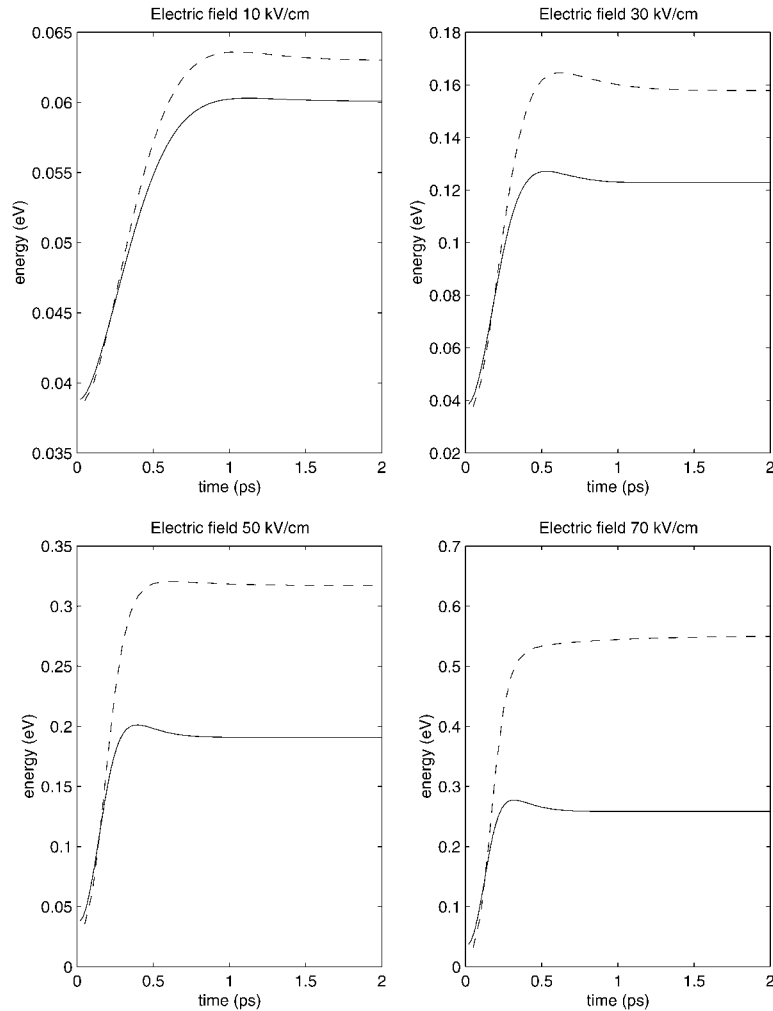


Figure 7. Energy (eV) versus electric field (kV/cm) in the parabolic band case (dashed line) and for the Kane dispersion relation.

The doping profile is regularized according to the function

$$n_0(x) = n_0 - d_0 \left(\tanh \frac{x - x_1}{s} - \tanh \frac{x - x_2}{s} \right)$$

where $s = 0.01 \mu\text{m}$, $n_0 = n_0(0)$, $d_0 = n_0(1 - N_D/N_D^+)/2$, $x_1 = 0.1 \mu\text{m}$, and $x_2 = x_1 + L_c$ with L_c channel length. The total length of the device is $L = L_c + 0.2 \mu\text{m}$. In Figure 9 the doping profile for the test case 1 is plotted.

A grid with 400 nodes has been used. The stationary solution is reached within a few picoseconds (about five), after a short transient with wide oscillations.

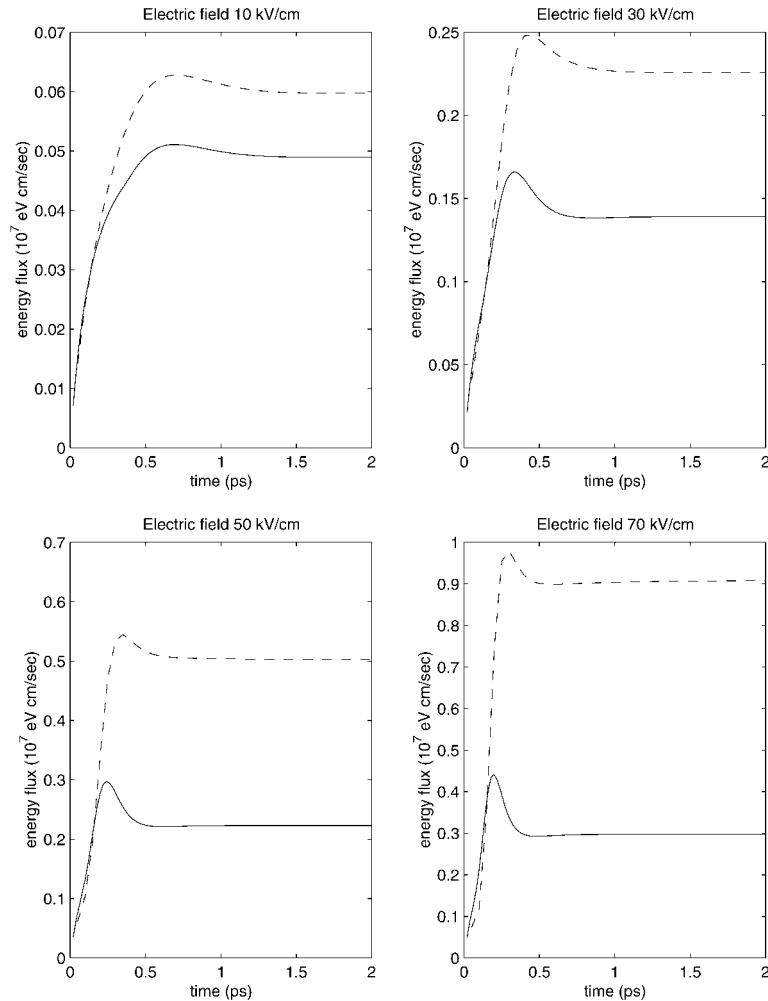


Figure 8. Energy flux (eV cm/s) versus electric field (kV/cm) in the parabolic band case (dashed line) and for the Kane dispersion relation.

As the first case we consider the test problem 1 (length of the channel $0.4\ \mu\text{m}$) with $V_b = 2\ \text{V}$. In Figures 10–13 the time-dependent solution and in Figure 14 (continuous line) the stationary solution (after 5 ps) are plotted. At variance with the numerical results obtained in Reference [10] for the parabolic case by using a quadratic closure in δ , our numerical solutions do not present irregularities. This can be probably ascribed to the absence of the non-linearities in the dissipative variables.

If we compare the results with those reported in Reference [34] (Figures 1–4) and obtained by solving with the Monte Carlo method the Boltzmann–Poisson system, there is a good agreement in all the variables W , V and S .

The simulation for the parabolic band approximation is also shown (Figure 14 dashed line), but it is evident, like in the bulk case, that the results are rather poor.

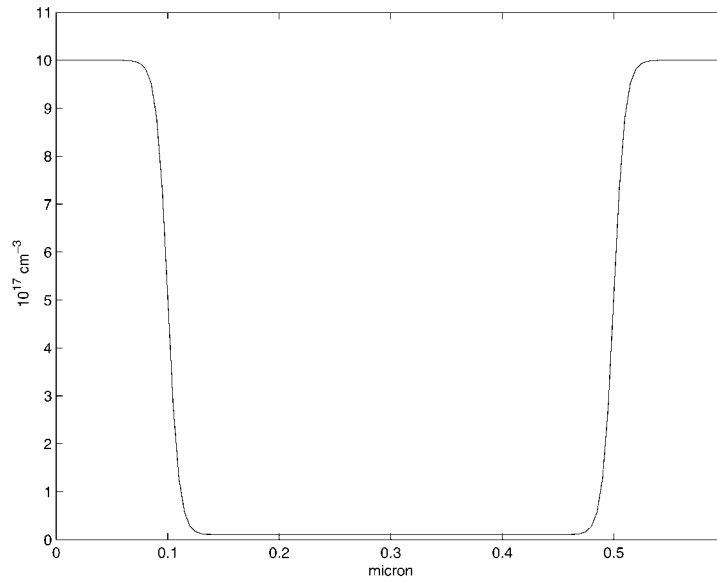


Figure 9. Doping profile for the test case 1.

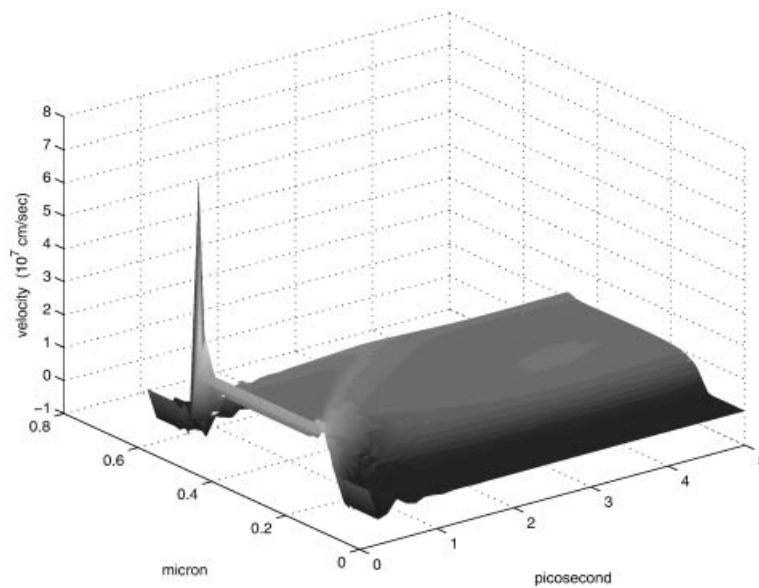


Figure 10. Time-dependent numerical result for the velocity of the test case 1 with the Kane dispersion relation.

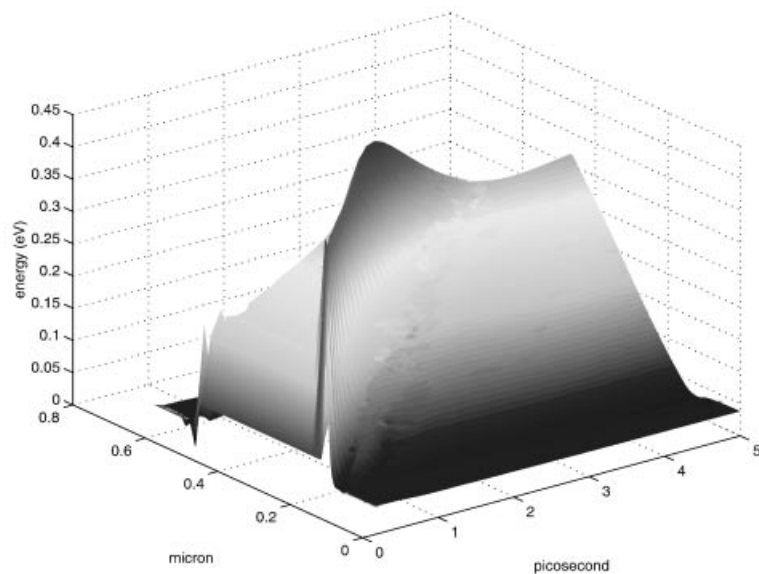


Figure 11. Time-dependent numerical result for the energy of the test case 1 with the Kane dispersion relation.

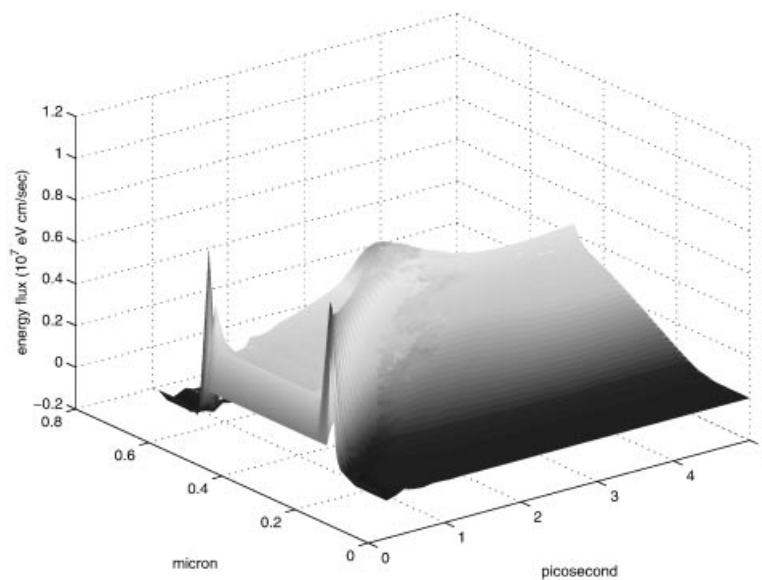


Figure 12. Time-dependent numerical result for the energy flux of the test case 1 with the Kane dispersion relation.

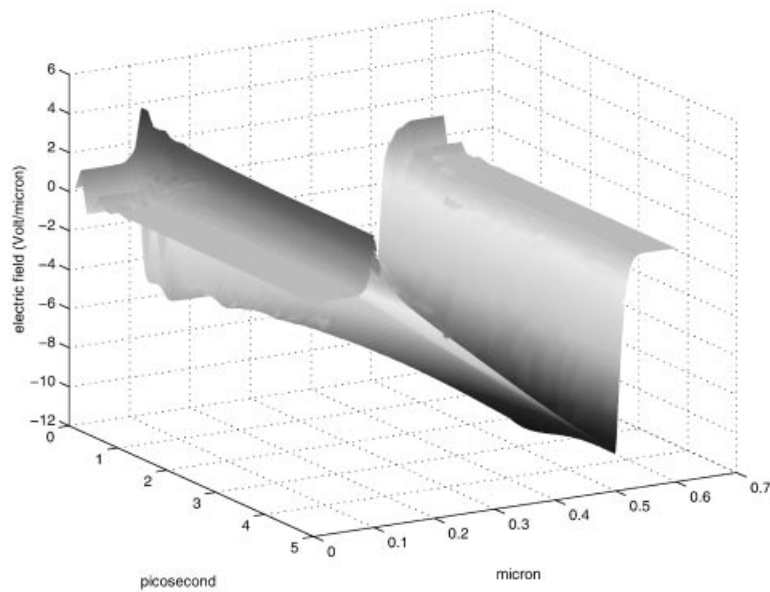


Figure 13. Time-dependent numerical result for the electric field of the test case 1 with the Kane dispersion relation.

The other test cases have been numerically integrated with $V_b = 1$ V (Figures 15 and 16). For these cases we have no Monte Carlo data, at our disposal, but the behaviour of the solution looks again physically reasonable and encouraging: the spurious spike across the second junction is here less apparent than several other hydrodynamical models. The results with the parabolic band are again rough when compared with those obtained in the non-parabolic case.

APPENDIX: SUMMARY OF THE CLOSURE RELATIONS

Here for the sake of completeness we summarize up to first order in δ all the constitutive equations needed for closing the balance equations (9), (11)–(13). For more details and for the second-order corrections see References [16, 17].

Concerning the tensor U^{ij} , F^{ij} and G^{ij} , up to first order we have

$$U^{ij} = U^{(0)} \delta^{ij} \quad (\text{A1})$$

$$F^{ij} = F^{(0)} \delta^{ij} \quad (\text{A2})$$

$$G^{ij} = G^{(0)} \delta^{ij} \quad (\text{A3})$$

with

$$U^{(0)} = \frac{2}{3d_0} \int_0^\infty [\mathcal{E}(1 + \alpha\mathcal{E})]^{3/2} \exp(-\lambda^{W(0)}\mathcal{E}) d\mathcal{E} \quad (\text{A4})$$

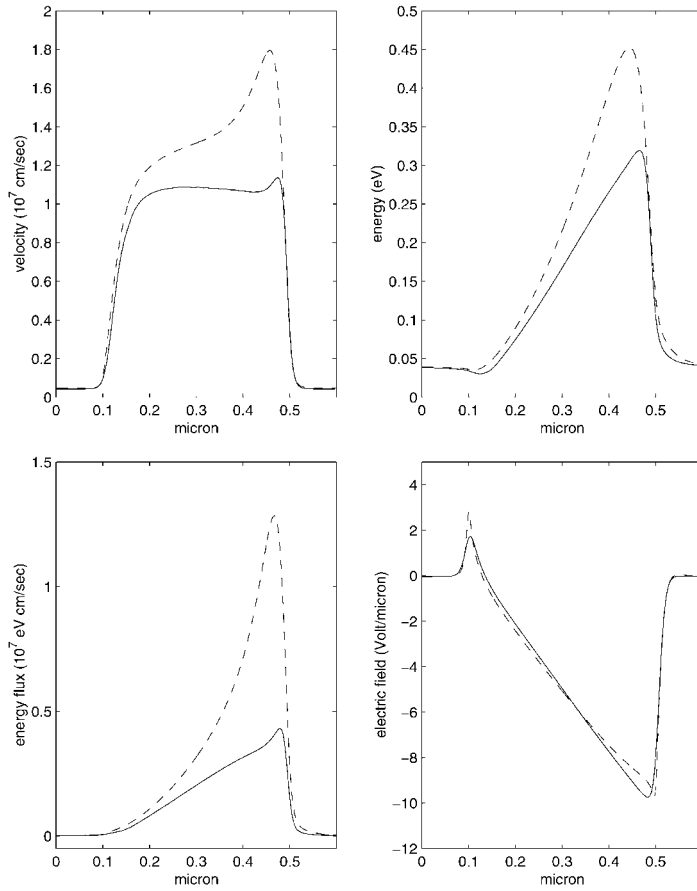


Figure 14. Numerical results of the test case 1 after 5p in the parabolic band case (dashed line) and for the Kane dispersion relation (continuous line).

$$F^{(0)} = \frac{2}{3m^*d_0} \int_0^\infty \exp(\lambda^{W(0)}\mathcal{E}) \frac{\mathcal{E}[\mathcal{E}(1 + \alpha\mathcal{E})]^{3/2}}{1 + \alpha\mathcal{E}} d\mathcal{E} \tag{A5}$$

$$G^{(0)} = \frac{1}{nm^*d_0} \int_0^\infty \exp(-\lambda^{W(0)}\mathcal{E}) \left(1 + \frac{2}{3(1 + 2\alpha\mathcal{E})}\right) \mathcal{E}^{3/2} \sqrt{1 + \alpha\mathcal{E}} d\mathcal{E} \tag{A6}$$

The production terms are the sum of the term due to the elastic scatterings (acoustic phonon scattering) and that due to inelastic phonon scatterings.

Concerning the acoustic phonon scattering, the contribution to the energy balance equation is zero while the production matrix $C^{(ac)} = (c_{ij}^{(ac)})$ is given by

$$C^{(ac)} = A^{(ac)}B$$

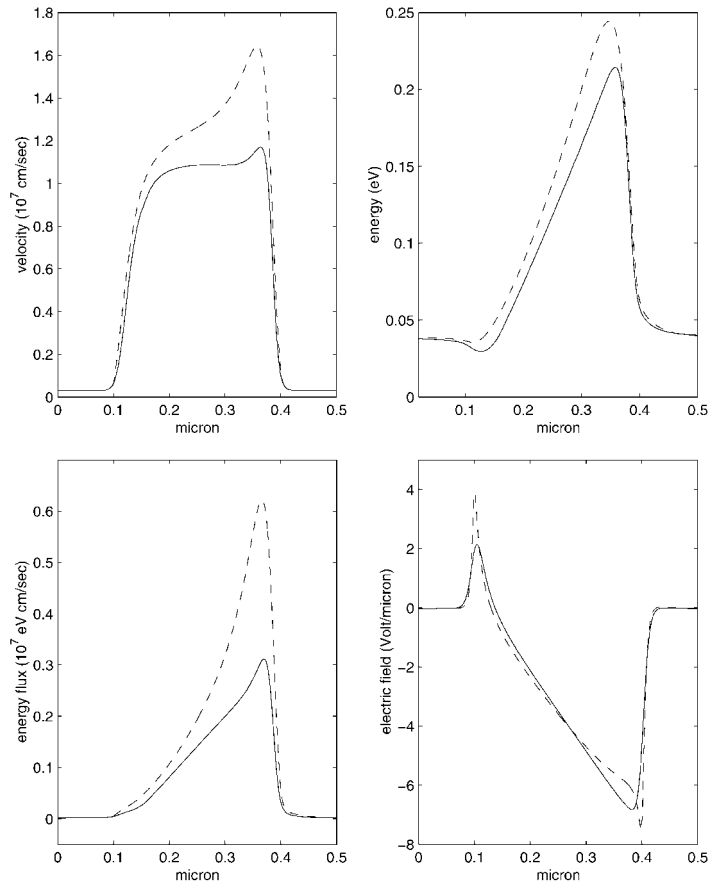


Figure 15. Numerical results of the test case 2 after 5 p in the parabolic band case (dashed line) and for the Kane dispersion relation (continuous line).

The coefficients b_{ij} of the matrix B are given by

$$b_{11} = \frac{a_{22}}{\Delta}, \quad b_{12} = -\frac{a_{12}}{\Delta}, \quad b_{22} = \frac{a_{11}}{\Delta}$$

with

$$a_{11} = -\frac{2p_0}{3m^*d_0}, \quad a_{12} = -\frac{2p_1}{3m^*d_0}, \quad a_{22} = -\frac{2p_2}{3m^*d_0}$$

and

$$\Delta = a_{11}a_{22} - a_{12}^2$$

d_k and p_k being

$$d_k = \int_0^\infty \mathcal{E}^k \sqrt{\mathcal{E}(1 + \alpha\mathcal{E})} (1 + 2\alpha\mathcal{E}) \exp(-\lambda^{W(0)}\mathcal{E}) d\mathcal{E}$$

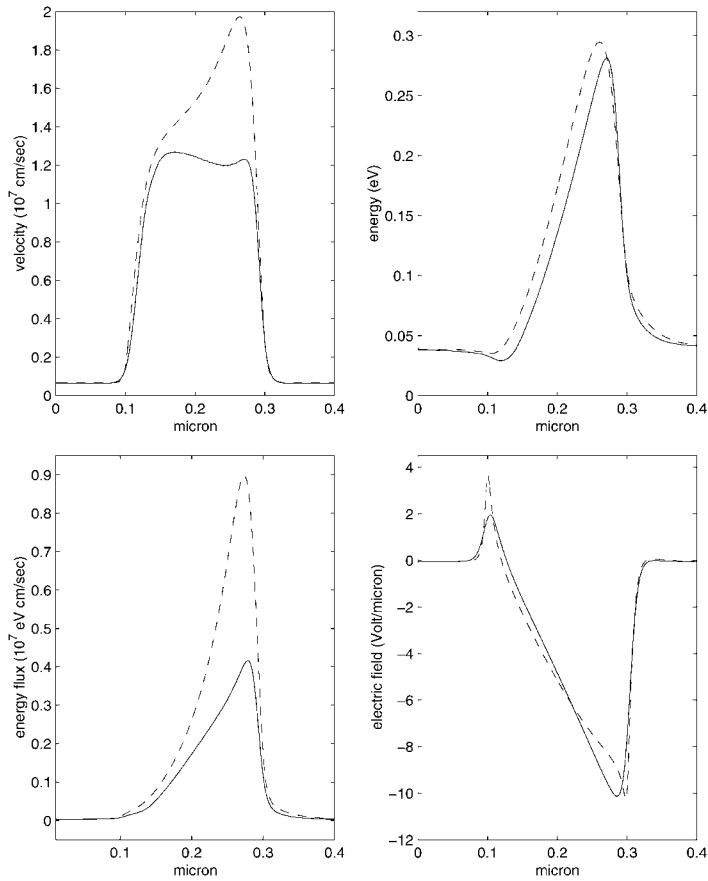


Figure 16. Numerical results of the test case 3 after 5p in the parabolic band case (dashed line) and for the Kane dispersion relation (continuous line).

$$p_k = \int_0^\infty \frac{[\mathcal{E}(1 + \alpha\mathcal{E})]^{3/2} \mathcal{E}^k}{1 + 2\alpha\mathcal{E}} \exp(-\lambda^{W(0)}\mathcal{E}) d\mathcal{E}$$

The coefficients of the matrix $A^{(ac)}$ read as

$$a_{11}^{(ac)} = \frac{\bar{K}_{ac}}{d_0} \int_0^\infty \mathcal{E}^2(1 + \alpha\mathcal{E})^2(1 + 2\alpha\mathcal{E}) \exp(-\lambda^{W(0)}\mathcal{E}) d\mathcal{E} \tag{A7}$$

$$a_{12}^{(ac)} = \frac{\bar{K}_{ac}}{d_0} \int_0^\infty \mathcal{E}^3(1 + \alpha\mathcal{E})^2(1 + 2\alpha\mathcal{E}) \exp(-\lambda^{W(0)}\mathcal{E}) d\mathcal{E} \tag{A8}$$

$$a_{21}^{(ac)} = \frac{\bar{K}_{ac}}{m^*d_0} \int_0^\infty \mathcal{E}^3(1 + \alpha\mathcal{E})^2 \exp(-\lambda^{W(0)}\mathcal{E}) d\mathcal{E} \tag{A9}$$

$$a_{22}^{(ac)} = \frac{\bar{K}_{ac}}{m^* d_0} \int_0^\infty \mathcal{E}^4 (1 + \alpha \mathcal{E})^2 \exp(-\lambda^{W(0)} \mathcal{E}) d\mathcal{E} \quad (\text{A10})$$

where

$$\bar{K}_{ac} = \frac{8\pi\sqrt{2}(m^*)^{3/2}K_{ac}}{3\hbar^3}, \quad K_{ac} = \frac{k_B T_L \Xi_d^2}{4\pi^2 \hbar \rho v_s^2}$$

Concerning the non-polar phonon scattering the production term of the energy balance equation is given by

$$C_W = \sum_{A=1}^6 C_{W_A}$$

where for each valley

$$C_{W_A} = \frac{3}{2} \frac{\bar{K}_{np}}{d_0} \sum_{\pm} \left(n_B + \frac{1}{2} \mp \frac{1}{2} \right) \left[\exp\left(\pm \frac{\hbar\omega_{np}}{k_B T_L} \mp \lambda^{W(0)} \hbar\omega_{np} \right) - 1 \right] \eta^\pm \quad (\text{A11})$$

with

$$\eta^\pm = \int_{\hbar\omega_{np}H(1\mp 1)}^\infty \mathcal{E} \mathcal{N}_\pm \sqrt{\mathcal{E}(1 + \alpha \mathcal{E})} (1 + 2\alpha \mathcal{E}) \exp(-\lambda^{W(0)} \mathcal{E}) d\mathcal{E} \quad (\text{A12})$$

$$\mathcal{N}_\pm = \sqrt{(\mathcal{E} \pm \hbar\omega_{np}) [1 + \alpha(\mathcal{E} \pm \hbar\omega_{np})] [1 + 2\alpha(\mathcal{E} \pm \hbar\omega_{np})]} \quad (\text{A13})$$

and

$$\bar{K}_{np} = \frac{8\pi\sqrt{2}(m^*)^{3/2}K_{np}}{3\hbar^3}, \quad K_{np} = Z_f \frac{(D_t K)^2}{8\pi^2 \rho \omega_{np}}$$

H is the Heaviside function

$$H(x) = \begin{cases} 1 & \text{if } x > 0 \\ 0 & \text{otherwise} \end{cases}$$

The coefficients of the production matrix $C^{(np)} = (c_{ij}^{(np)})$ are given by

$$c_{ij}^{(np)} = \sum_{A=1}^6 c_{A_{ij}}^{(np)}$$

For each valley one has

$$C^{(np)} = A^{(np)} B$$

where the matrix $A^{(np)}$ has components

$$a_{11}^{np} = \frac{\bar{K}_{np}}{d_0} \sum_{\pm} \left(n_B + \frac{1}{2} \mp \frac{1}{2} \right) \int_{\hbar\omega_{np}H(1\mp 1)}^\infty \mathcal{N}_\pm \mathcal{E}^{3/2} (1 + \alpha \mathcal{E})^{3/2} \exp(-\lambda^{W(0)} \mathcal{E}) d\mathcal{E} \quad (\text{A14})$$

$$a_{12}^{np} = \frac{\bar{K}_{np}}{d_0} \sum_{\pm} \left(n_B + \frac{1}{2} \mp \frac{1}{2} \right) \int_{\hbar\omega_{np}H(1\mp 1)}^{\infty} \mathcal{N}_{\pm} \mathcal{E}^{5/2} (1 + \alpha \mathcal{E})^{3/2} \exp(-\lambda^{W(0)} \mathcal{E}) d\mathcal{E} \quad (\text{A15})$$

$$a_{21}^{np} = \frac{\bar{K}_{np}}{m^* d_0} \sum_{\pm} \left(n_B + \frac{1}{2} \mp \frac{1}{2} \right) \int_{\hbar\omega_{np}H(1\mp 1)}^{\infty} \mathcal{N}_{\pm} \frac{\mathcal{E}^{5/2} (1 + \alpha \mathcal{E})^{3/2}}{1 + 2\alpha \mathcal{E}} \exp(-\lambda^{W(0)} \mathcal{E}) d\mathcal{E} \quad (\text{A16})$$

$$a_{22}^{np} = \frac{\bar{K}_{np}}{m^* d_0} \sum_{\pm} \left(n_B + \frac{1}{2} \mp \frac{1}{2} \right) \int_{\hbar\omega_{np}H(1\mp 1)}^{\infty} \mathcal{N}_{\pm} \frac{\mathcal{E}^{7/2} (1 + \alpha \mathcal{E})^{3/2}}{1 + 2\alpha \mathcal{E}} \exp(-\lambda^{W(0)} \mathcal{E}) d\mathcal{E} \quad (\text{A17})$$

ACKNOWLEDGEMENTS

This work has been partially supported by MURST, *Fondi 60%* and project *Problems in kinetic theory*, by CNR project *Modelli matematici per semiconduttori. Progetto speciale: metodi matematici in fluidodinamica e dinamica molecolare*, grant number 96.03855.CT01 and by TMR program *Asymptotic methods in kinetic theory*, grant number ERBFMRXCT 970157.

REFERENCES

1. Blotekjaer K. Transport equations for electron in two-valley semiconductors. *IEEE Transactions on Electron Devices* 1970; **ED-17**:38–47.
2. Baccarani G, Wordeman MR. An investigation on steady-state velocity overshoot in silicon. *Solid-State Electronics* 1982; **29**:970–977.
3. Anile AM, Muscato O. Improved hydrodynamical model for carrier transport in semiconductors. *Physical Review B* 1995; **51**:16,728–16,740.
4. Selberherr S. *Analysis and Simulation of Semiconductor Devices*. Springer: Wien, New York, 1984.
5. Hänsch W. *The Drift-Diffusion Equation and its Applications in MOSFET Modeling*. Springer: Wien, 1991.
6. Markowich P, Ringhofer CA, Schmeiser C. *Semiconductor Equations*. Springer: Wien, 1990.
7. Chen D, Kan EC, Ravaioli U, Shu C-W, Dutton R. An improved energy-transport model including non-parabolicity and non-maxwellian distribution effects. *IEEE on Electron Device Letters* 1992; **13**:26–28.
8. Lyumkis E, Polsky B, Shir A, Visocky P. Transient semiconductor device simulation including energy balance equation. *Compel* 1992; **11**:311–325.
9. Abdallah NB, Degond P. On a hierarchy of macroscopic models for semiconductors. *Journal of Mathematical Physics* 1996; **37**:3308–3333.
10. Anile AM, Romano V, Russo G. Extended hydrodynamical model of carrier transport in semiconductors. *SIAM Journal on Applied Mathematics* 2000; **61**(1):74–101.
11. Müller I, Ruggeri T. *Rational Extended Thermodynamics*. Springer: Berlin, 1998.
12. Jou D, Casas-Vazquez J, Lebon G. *Extended Irreversible Thermodynamics*. Springer: Berlin, 1993.
13. Levermore CD. Moment closure hierarchies for kinetic theories. *Journal of Statistical Physics* 1996; **83**:331–407.
14. Anile AM, Pennisi S. Thermodynamic derivation of the hydrodynamical model for charge transport in semiconductors. *Physical Review B* 1992; **46**:13,186–13,193.
15. Anile AM, Romano V, Russo G. Hyperbolic hydrodynamical model of carrier transport in semiconductors. *VLSI Design* 1998; **8**(1–4):521–525.
16. Anile AM, Romano V. Non parabolic band transport in semiconductors: closure of the moment equations. *Continuum Mechanics and Thermodynamics* 1999; **11**:307–325.
17. Romano V. Non parabolic band transport in semiconductors: closure of the production terms in the moment equations. *Continuum Mechanics and Thermodynamics* 1999; **12**:31–51.
18. Anile AM, Muscato O, Romano V. Moment equations with the maximum entropy closure for carrier transport in semiconductor devices: validation in bulk silicon. *VLSI Design* 2000; **10**:335–354.
19. Ashcroft NW, Mermin ND. *Solid State Physics*. Saunders College Publishing International Edition: Philadelphia, 1976.
20. Jacoboni C, Reggiani L. The Monte Carlo method for the solution of charge transport in semiconductors with application to covalent materials. *Review of Modern Physics* 1983; **55**:645–705.
21. Jacoboni C, Lugli P. *The Monte Carlo Method for Semiconductor Device Simulation*, Springer: Wien, New York, 1989.

22. Tomizawa K. *Numerical Simulation of Sub Micron Semiconductor Devices*. Artech House: Boston, 1993.
23. Dreyer W. Maximization of the entropy in non-equilibrium. *Journal of Physics A: Mathematics and General* 1987; **20**:6505–6517.
24. Fischetti M, Laux S. Monte Carlo study of electron transport in silicon inversion layer. *Physical Review B* 1993; **48**:232–244.
25. Tang T-W, Ramaswamy S, Nam J. An improved hydrodynamical transport model for silicon. *IEEE on Electron Devices* 1993; **40**:1469–1477.
26. Fischetti M, Laux S. *DAMOCLES Theoretical Manual*. Copyright IBM Corporation, 1994.
27. Toro EF. *Riemann Solvers and Numerical Methods for Fluid Dynamics*. Springer: Berlin, 1997.
28. LeVeque RJ. *Numerical Methods for Conservation Laws*. Birkhäuser: Zürich, 1992.
29. Liotta F, Romano V, Russo G. Central schemes for systems of balance laws. *International Series of Numerical Mathematics* 1999; **130**:651–660.
30. Liotta F, Romano V, Russo G. Central schemes for balance laws of relaxation type. *SIAM Journal on Numerical Analysis* 2000; **38**:1337–1356.
31. Nessyahu H, Tadmor E. Non-oscillatory central differencing for hyperbolic conservation law. *Journal of Computational Physics* 1990; **87**:408–463.
32. Romano V, Russo G. Numerical solutions for hydrodynamical models of semiconductors. *M³AS* 2000; **10**:1099–1120.
33. Fatemi E, Jerome J, Osher S. Solution of hydrodynamic device model using high-order nonoscillatory shock capturing algorithms. *IEEE Transaction on Computer-Aided Design* 1991; **10**:232–398.
34. Ramaswamy S, Tang T-W. Comparison of semiconductor transport model using a Monte Carlo consistency test. *IEEE Electron Devices* 1994; **41**:76–83.